Ultrasonic enrichment of microspheres for ultrasensitive biomedical analysis in confocal laser-scanning fluorescence detection

M. Wiklund[a)]
Biomedical and X-Ray Physics, Royal Institute of Technology, AlbaNova, SE-106 91 Stockholm, Sweden

J. Toivonen
Institute of Biomedicine, Laboratory of Biophysics, University of Turku, Tykistökatu 6, Turku FIN-20520, Finland

M. Tirri
Institute of Biomedicine, Laboratory of Biophysics, University of Turku, Tykistökatu 6, Turku FIN-20520, Finland

P. Hänninen
Institute of Biomedicine, Laboratory of Biophysics, University of Turku, Tykistökatu 6, Turku FIN-20520, Finland

H. M. Hertz
Biomedical and X-Ray Physics, Royal Institute of Technology, AlbaNova, SE-106 91 Stockholm, Sweden

(Received 10 February 2004; accepted 26 April 2004)

An ultrasonic particle concentrator based on a standing-wave hemispherical resonator is combined with confocal laser-scanning fluorescence detection. The goal is to perform ultrasensitive biomedical analysis by concentration of biologically active microspheres. The standing-wave resonator consists of a 4 MHz focusing ultrasonic transducer combined with the optically transparent plastic bottom of a disposable 96-well microplate platform. The ultrasonic particle concentrator collects suspended microspheres into dense, single-layer aggregates at well-defined positions in the sample vessel of the microplate, and the fluorescence from the aggregates is detected by the confocal laser-scanning system. The biochemical properties of the system are investigated using a microsphere-based human thyroid stimulating hormone assay. © *2004 American Institute of Physics.* [DOI: 10.1063/1.1763226]

I. INTRODUCTION

Immunoassay-based techniques for quantification of biomolecules are becoming increasingly important in clinical diagnostics and proteomics research. In the present paper we demonstrate a high-sensitivity microsphere-based immunoassay detection technique by combining confocal laser scanning fluorescence detection and ultrasonic trapping for sample enrichment. The properties of the ultrasonic standing-wave system for ultrasensitive detection are investigated theoretically and experimentally. The goal is to enrich microspheres into single, dense layers matching the laser focus scanning regions of the optical detection system. The performance of the system is experimentally demonstrated using a microsphere-based thyroid stimulating hormone assay (TSH assay) (Ref. 1) as the model assay.

Today, there exists numerous different fluorescence-based microsphere-enhanced immunoassay techniques. In a typical assay, antibody-coated microspheres are used to bind target molecules in the sample, and quantification of the binding reaction reveals the amount of target molecules. Recently, single-step homogeneous assays have gained attention due to the ability to perform fast and simple analysis, e.g., in suspension array technology (SAT).[2] Single-step laser-scanning applications include ''macro-confocal'' laser scanning fluorescence detection.[3–6] Here, a 100 μm axially elongated laser focus is used for measuring the microsphere fluorescence near the bottom of the reaction vessel. Furthermore, a very sensitive laser-scanning method is two-photon excitation (TPX) technology.[7] Here, the fluorescence of two-photon excitation from one particle at a time is measured in a small confocal volume element ($\sim$1 fl). Ultrasensitive methods based on statistical analysis of intensity fluctuations are fluorescence correlation spectroscopy (FCS) (Ref. 8) and fluorescence-intensity distribution analysis (FIDA).[9] Here, the analyte is most often observed directly in a confocal volume element, but both FCS and FIDA have also been used with the nanoparticle immunoassay (NPIA) for enhanced signal to noise ratio of the assay.[10,11]

Standing-wave ultrasonic manipulation of suspended particles has been used for different agglutination, separation, manipulation, or processing purposes.[12–15] Biological applications include cell or bacteria manipulation (characterization, concentration, or filtering).[16–18] Furthermore, ultrasonic traps have been combined with microsphere-based immunoagglutination assays for enhancement of latex agglutination tests (LATs) (Refs. 19 and 20) and for size-selective separation in capillaries for biochemical analysis.[21]

In the present paper standing-wave ultrasonic is used for microsphere-based sample enrichment aiming at ultrasensi-

a)Electronic mail: martin@biox.kth.se

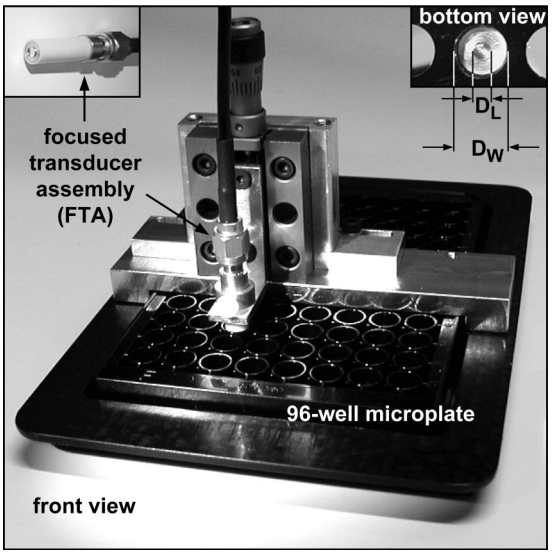

FIG. 1. Front and bottom view of the ultrasonic particle concentrator (UPC), that consists of the focused transducer assembly (FTA) combined with the 96-well microplate. Here, the diameters of the acoustic lens (D_L) and a well bottom (D_W) are 2.5 mm and 6.3 mm, respectively.

tive separation-free laser-fluorescence immunoassay detection. Our ultrasonic particle concentrator (UPC) is based on a standing-wave acoustic cavity, which is formed between a miniature focused transducer assembly (FTA) and the transparent optical window of the bottom of a commercially available disposable 96-well microplate. The system is shown in Fig. 1. Since the target molecules are immobilized on the microspheres, sample enrichment is performed by microsphere concentration. Thus, the combined ultrasound-fluorescence method is an ultrasensitive single-step detection technique based on relatively inexpensive instrumentation that exists in many laboratories. We analyze, theoretically and experimentally, the stability of the acoustic cavity as well as of the microsphere trapping. Furthermore, we report initial experiments with TSH assay suggesting a theoretical detection limit of about 0.003 mIU/L or even lower, corresponding to 20 fM for this assay. This is an application of ultrasonic particle enrichment for ultrasensitive single-step laser-fluorescence analysis.

II. THEORETICAL BACKGROUND

In this section we describe the principles of standing-wave ultrasonic manipulation of suspended spherical objects. The geometrical conditions for resonance and mode stability are discussed for the hemispherical standing-wave system that consists of the focused transducer assembly (FTA) and the 96-well microplate, forming an ultrasonic particle concentrator (UPC). The UPC is illustrated in Fig. 2. The experimental setup of the UPC and the detection system is described in more detail in Sec. III.

A. Principles of standing-wave ultrasonic manipulation

The theory of acoustic radiation forces in a standing-wave field has been derived by several authors.[22,23] Basically, a solid sphere in a suspension will be trapped in the

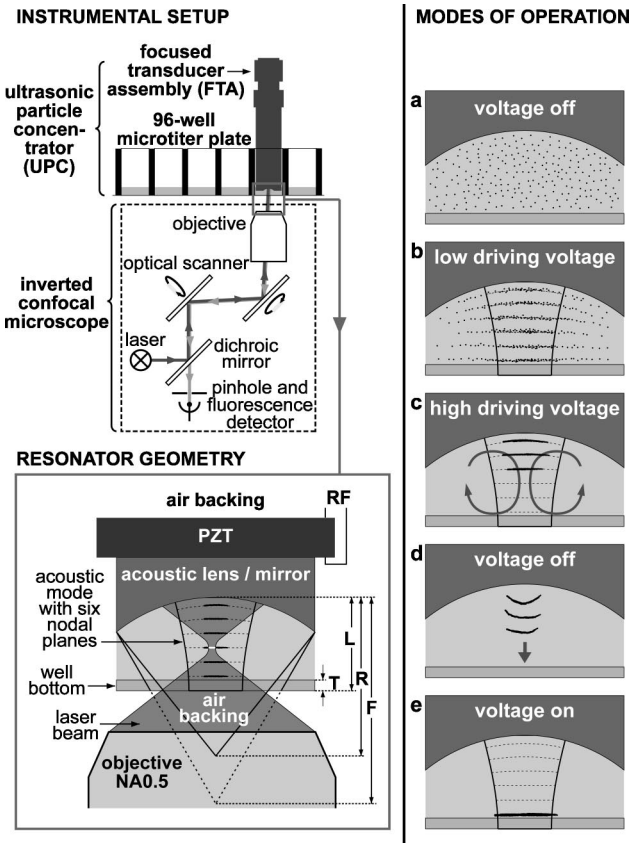

FIG. 2. Left side: Schematic illustration of the experimental arrangement for the ultrasonic particle concentrator (UPC) and the confocal laser-scanning fluorescence detection system in an inverted confocal microscope. Right side: The different modes of operation (a)–(e).

pressure nodes of the standing wave. The acoustic radiation force on a spherical object in an arbitrary standing-wave field can be written as[24]

$$\mathbf{F} = -2\pi r^3 \cdot \nabla \left(a_1 \cdot \frac{\langle p^2 \rangle}{3\rho c^2} - a_2 \cdot \frac{\rho \langle v^2 \rangle}{2} \right), \tag{1}$$

where r is the radius of the sphere, $\langle p^2 \rangle$ and $\langle v^2 \rangle$ are the mean-square fluctuations of the pressure and the velocity of the acoustic field at the point where the sphere is located, ρ is the density of the medium, and c is the speed of sound in the medium. The factors a_1 and a_2 are dimensionless corrections taking compressibility of the sphere into account, defined as

$$a_1 = 1 - \frac{\rho c^2}{\rho_s c_s^2}, \quad a_2 = \frac{2(\rho_s - \rho)}{2\rho_s + \rho}, \tag{2}$$

where ρ_s and c_s are the density and the speed of sound in the sphere, respectively. In the case of a single-axis resonator, a suspended particle will first move in the axial direction, where the radiation force is the highest. When it approaches the pressure nodal plane, the lateral component of the radiation force will further move the particle towards the symmetry axis of the standing-wave field. In plane resonator geometries, the lateral forces are most often weak in comparison to the axial forces. However, if several suspended particles are concentrated in the pressure nodal plane, they experience forces from the scattered acoustic field originating from par-

ticles at close distance. This force, often referred to as Bjerknes force,[23] is attractive for particles oriented at right angles to the incident acoustic beam and is one of the reasons that particles may form single-layer, dense aggregates in the pressure nodal plane. Furthermore, if the resonator geometry is focusing, the lateral forces are higher.[25] Even a slightly focusing geometry is important for mode stability, for easy alignment and for minimizing the energy losses out of the resonant cavity hosting the standing wave. A calculation of the geometrical parameters of the standing-wave resonator used in the experiment is given in the following section.

High acoustic intensities can also induce fluid motion via acoustic streaming. The acoustic streaming of interest for the work presented here is the large-scale streaming,[26] which is generated by the attenuation of the acoustic wave. A typical streaming geometry in our cavity is of rotational character, having one direction on the cavity axis and the other direction near the cavity boundary, and the magnitude can be several centimeters per second [cf. Fig. 2(c)]. If the fluid motion is large enough, the viscous drag force ($F_v = 6\pi\eta r u$, where η is the viscosity of the liquid medium and u is the fluid speed) might exceed the acoustic force and destroy the trap.

B. Resonator geometry

In this section, a motivation of the choice of geometrical parameters for the ultrasonic resonator is given, based on theoretical calculations. The goal is to generate a focusing standing-wave mode for microsphere enrichment into the pressure nodes, both axially and laterally. The hemispherical resonator geometry is shown in the lower left part of Fig. 2. Basically, it consists of an air-backed plane piezoceramic disk, an acoustic lens made of aluminum or brass, the water-based medium, and an air-backed plane polystyrene (PS) layer (i.e., the bottom of a sample vessel in the 96-well microplate). More practical details of the experimental setup are given in the following section. The incident acoustic wave generated by the transducer is focused by the acoustic lens into the sample vessel. (The standing wave is formed by multiple reflections is the PS bottom and in the acoustic lens which also acts as a mirror.) The total pressure reflection coefficient (r_p) of a thin layer is given by[27]

$$r_p = \frac{Z_R(Z_B - Z_W) + i(Z_R^2 - Z_W Z_B)\tan(k_R L_R)}{Z_R(Z_B + Z_W) + i(Z_R^2 + Z_W Z_B)\tan(k_R L_R)}, \tag{3}$$

where k_R is the wave number in the reflector, L_R is the reflector thickness, and Z_W, Z_R, and Z_B are the specific acoustic impedances of the water, reflector. (PS), and backing (air) layers, respectively. The real part of r_p gives the amplitude ratio between the incident and reflected waves, which has a maximum value when the imaginary part of r_p is zero. Maximum r_p and zero phase shift are obtained when L_R is an odd multiple of $\lambda/4$. For example, a $\lambda/4$ plate of PS ($Z_R \approx 1.6 \times Z_W \approx 5600 \times Z_B$) (Ref. 28) has a maximum pressure reflection coefficient >0.9997. Thus, despite the similar magnitudes of the acoustic impedances of water and PS, a thickness-matched microplate bottom has high reflectivity due to the very low impedance of air.

For a given combination of the thicknesses of the acoustic lens and the PS bottom of the microplate, the resonances can be found either by tuning the frequency of the transducer, or by tuning the distance between the lens and the PS bottom. Here, the latter method was applied. The performance of a layered resonator in a plane-parallel geometry can be calculated by the impedance transfer model described by Hill *et al.*[29] The qualitative results from such a calculation applied to the work presented here predict the distance L (cf. Fig. 2) between the acoustic lens and the PS bottom of the microplate. Each resonant value of L for a fixed frequency is separated by $\lambda/2$, and the distance between the pressure nodes in the standing wave is also separated by $\lambda/2$ for a certain value of L. However, since the lens and PS layers are not perfectly matched to the zero-phase-shift criterion, the exact positions of the pressure nodes relative to the boundaries of the water-based sample layer are more difficult to predict. Furthermore, the geometry in this work is hemispherical, which can influence the distance between the nodes. Xie *et al.* have shown that for a hemispherical resonator the distance between two resonant states is slightly longer than $\lambda/2$.[25] This is valid when both the reflector diameter and the resonator length are comparable to the wavelength. However, we have not observed such deviations in our experiments. It should be noted that we have chosen to define the resonator length as the distance from the curved surface of the acoustic lens to the surface between the PS layer and the backing medium (air). The reason is that those two surfaces are the primary contributors to the back-reflected acoustic intensity for each round trip in the resonator, since the bottom reflector is made of plastic.

Another important condition for the resonator geometry is related to the spatial mode shape of the standing wave. A stability condition for a Gaussian wave in a hemispherical resonator is that the resonator length (L) should be less than the radius of curvature of the curved mirror (R),[30]

$$L < R. \tag{4}$$

Furthermore, to minimize the lateral losses out of the resonant cavity, the mode radii at the mirrors must be less than the mirror radii. The lateral mode radii at the mirrors in a hemispherical resonator are given by[30]

$$w_L = \left(\frac{\lambda^2 R^2 L}{\pi^2 (R - L)} \right)^{1/4}$$

and

$$w_B = \left(\frac{\lambda^2 L (R - L)}{\pi^2} \right)^{1/4} \tag{5}$$

where w_L and w_B are the mode radii at the curved mirror (the acoustic lens) and the plane mirror (the lower bottom surface), respectively, and λ is the wavelength in the medium. The mode radius w for a Gaussian mode is here defined as the radius where the amplitude is e^{-1} times the maximum amplitude. In Fig. 3, the ratio between the mode radii (w) and the lens radius ($D/2$) for the possible stable modes of the hemispherical resonator used in the experiments are calculated as a function of the ratio between the resonator axis

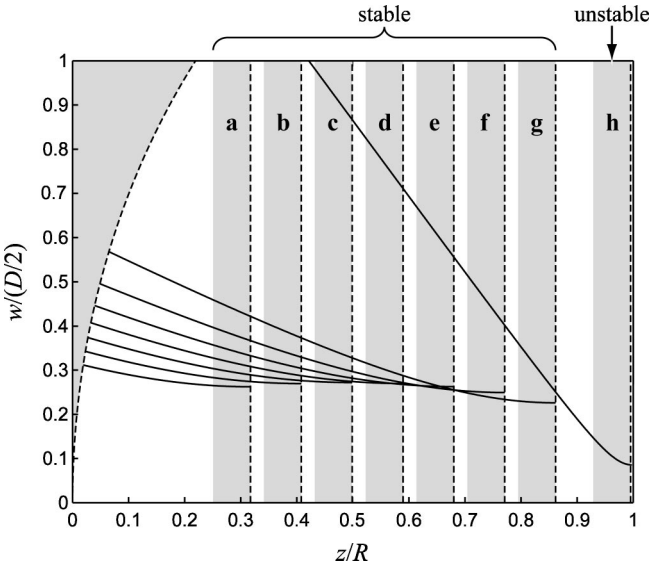

FIG. 3. Calculation of the resonant mode radii (w) along the resonator axis (z) in a hemispherical resonator, at eight different positions of the polystyrene (PS) reflector (a)–(h). The acoustic lens is fixed at $z=0$ and its reflecting surface is marked with the curved dotted line. The main reflecting surface of the PS layer (marked in gray) is marked with a straight dotted line. The lens diameter (D) is 2.5 mm, the radius of curvature of the lens (R) is 2.0 mm, and the wavelength (λ) is 360 μm. Here, seven different stable resonator lengths are possible (a)–(g), each separated by $\lambda/2$. If the resonator length (L) is close to the radius of curvature (R), e.g., position (h) in the diagram, the mode is too lossy and will not give resonance.

position (z) and the radius of curvature of the lens (R). The straight dotted lines are the positions of the back surface of the reflecting bottom of the microplate. The gray areas signify the thicknesses of the microplate PS bottom. In the calculation, the wavelength in the microplate bottom is scaled to the same wavelength as in the medium (water). The best observed experimental performance (with respect to the microsphere concentration efficiency) is when $w_L/(D/2)<0.5$ and $w_L/w_B<2$, which means that the mode radius should be less than half the lens radius and not too focusing. This corresponds to resonator lengths (L) of approximately half the radius of curvature (R) of the acoustic lens. In Fig. 3, the microplate positions (a)–(e) give the best performance, the positions (f)–(g) are tolerable, while the position (h) is unstable and lossy.

III. EXPERIMENTAL ARRANGEMENT

The experimental arrangement shown in Fig. 1 is illustrated schematically in the left part of Fig. 2. The system is built around a Zeiss Axiovert 10 inverted confocal microscope equipped with the 514.5 nm line from an Ar^+ laser, an optical scanner unit, a fluorescence filter set with a 550–600 nm bandpass emission filter and a single-photon-counting avalanche photodiode detector (type SPCM-AQ-131, PerkinElmer Optoelectronics, Canada). Optical sections were aquired with a Zeiss Plan-Neofluar 20×/0.50 NA/working distance 2.0 mm. The sample is placed in a disposable 96-well microplate (μCLEAR medium binding, Greiner GmbH, Germany) with a thin PS bottom (thickness 190 ± 20 μm) for inverted optical access. Each vessel in the microplate has

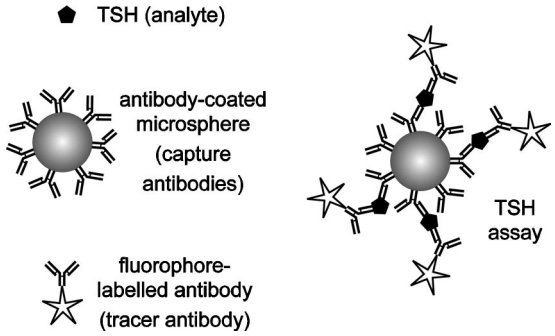

FIG. 4. The microsphere-based thyroid stimulating hormone (TSH) assay.

dimensions 6.35×11.0 mm (diameter×height), thus compatible for sample volumes up to 300 μl. The focused transducer assembly (FTA) is placed in the sample vessel from above by a high-precision vertical translation stage. The FTA consists of a plane air-backed lead zirconate titanate (PZT) ultrasonic transducer (thickness 0.5 mm, diameter 5.0 mm Pz26, Ferroperm, Denmark) combined with an acoustic lens/mirror. The transducer is driven at a frequency close to the thickness mode eigenfrequency of the piezoceramic disk (4.08 MHz). Two ring-shaped front and back brass electrodes, insulated with a teflon-layer, are attached to an electrical connector (type SMA) and to the piezoceramic disk by conducting epoxy, making the FTA device small and flexible (totally 5 mm×30 mm). In the experiments, two different acoustic lenses were used, an aluminum lens and a brass lens having dimensions 5.0 mm/2.5 mm (diameter), 4.0 mm/2.0 mm (radius of curvature) and 5.2 mm/2.9 mm (focal length), respectively. In the fluorescence measurements, the larger lens was used.

As a model assay to demonstrate the performance of the system, the human thyroid stimulating hormone (hTSH) (Ref. 1) was used cf. Fig. 4). The TSH assay consisted of 3.2 μm carboxy modified microspheres (Bangs Laboratories, Fishers, IN) coated with antibodies from clone 5404, $K_a=2\times10^{10}\,M^{-1}$ (Medix Biochemica, Espoo, Finland), a hTSH standard (Catalogue No. T0133, Scripps Laboratories, San Diego, CA) and tracer antibodies [succidinimidyl ester of the orange fluorescent dye BF 530 (Arctic Diagnostics Oy, Turku, Finland), linked to antibodies from clone 5409, $K_a=1\times10^{10}\,M^{-1}$ (Medix Biochemica, Espoo, Finland)]. The two different antibodies (microsphere bound and flourophore bound) were directed against two different epitopes of the TSH. The fluorescent dye of the tracer antibody had $\lambda_{ex}=530$ nm and $\lambda_{em}=552$ nm, and the 514.5 nm line of the Ar^+ laser was used for excitation. The buffer used when incubating the assay contained 50 mM Tris-HCl, 150 mM NaCl, 10 mM NaN_3, 0.5% BSA, and 0.01% Tween-20. In the fluorescence measurement, this buffer was exchanged to pure water.

IV. RESULTS

Each experiment was initiated by an alignment procedure to find a stable resonant state of the standing-wave ultrasonic trap. The FTA was gently placed in the sample vessel containing 50–150 μl of sample with microspheres. When a low voltage ($\sim10-20\,mV_{pp}$) was applied over the

transducer, the measured electrical impedance could be used to tune the resonator length L into a resonant state. At this voltage level, no noticeable movement of the suspended microspheres was observed. At resonance, a typical voltage drop of ~10%–15% was measured over the transducer. At the applied frequency of ~4.1 MHz, the axial width of a resonant state was of the order of one or a few micrometers, indicating a ''finesse'' of the order of 100. The distance between two consecutive resonant states was measured to 180 μm, which, together with the ''finesse,'' is in good agreement with the calculations using the Hill model[29] and the expected value of $\lambda/2$ in water at 4.1 MHz.

After the alignment, the voltage was raised to a higher value ($>1\ V_{pp}$) where movement and trapping of the microspheres into the pressure nodal planes occurred. Different resonator lengths were evaluated, and the most efficient and stable microsphere enrichment was observed when the resonator length was around half the radius of curvature of the acoustic lens, which is in good agreement with the calculations of the acoustic mode shape in Sec. II B. A typical number of chosen pressure nodes in the resonator were 4–7 for the 2 mm R lens and 8–15 for the 4 mm R lens. Here, the maximum lateral mode radius (at the lens surface) of the standing wave is less than half the lens radius, which gives low losses due to diffraction of the wave. Furthermore, the acoustic forces are of equal magnitude throughout the sample since the axial mode shape is less focusing.

In the right part of Fig. 2, the different modes of operation are illustrated for the smaller FTA (with 2 mm R lens). Here, the resonator length is chosen to contain six pressure nodes, which gives $L \approx 1.3$ mm. Initially, the microspheres are uniformly distributed in the sample (a). When a low voltage level is applied over the transducer ($<2\ V_{pp}$), the microspheres are concentrated into the pressure nodal planes, and further collected laterally towards the resonator axis (b). This is a rather slow process that typically takes several minutes before the maximum concentration is reached. If the transducer voltage is higher ($2-10\ V_{pp}$), the microspheres move faster and may be trapped in a few seconds, but acoustic streaming could also destroy the traps (c). Typically, the streaming is higher in the lower part of the cavity, putting the microspheres into torus-shaped streaming orbitals, going downwards in the center of the cavity and upwards at the periphery of the cavity. However, many of these microspheres are instead trapped in the upper pressure nodes (near the FTA), which are not destroyed by the streaming. If enough microspheres are trapped and packed in one nodal plane, the microsphere aggregate may sink relatively fast (~30–60 s) to the bottom of the vessel when the voltage is turned off (d). Then, there is a possibility to retrap all the microsphere aggregates in the lowest plane close to the bottom (e). Thus, in principle, all microspheres can be concentrated into a single horizontal layer near, but not on, the vessel bottom. This is suitable for combination with high-NA-objective confocal detection of the microsphere fluorescence. In Fig. 5, this mode of operation is demonstrated experimentally. Here, the PS bottom of the microplate is cut out and placed in a square-shaped cuvette to allow side view. The sample contains ~10^6 microspheres/mL of 4.5 μm fluorescent microspheres (Polyscience, PA). The smaller FTA (with 2 mm R lens) is driven at a high, streaming-inducing transducer voltage (~$10\ V_{pp}$), resulting in trapping only in the upper part of the resonator. In the images in Fig. 5, only the 3rd and higher nodes from the FTA are visible due to the concave shape of the acoustic lens. By turning on and off the acoustic intensity, the aggregates of trapped microspheres sink to the bottom and are finally retrapped in a large and dense disk in the lowest node, ~90 μm from the microplate bottom. When the microspheres once are trapped in dense and plane aggregates, they are easily manipulated (e.g., dropped and retrapped) due to the larger volume and to the internal forces between the spheres (Bjerknes forces) as discussed in Sec. II.

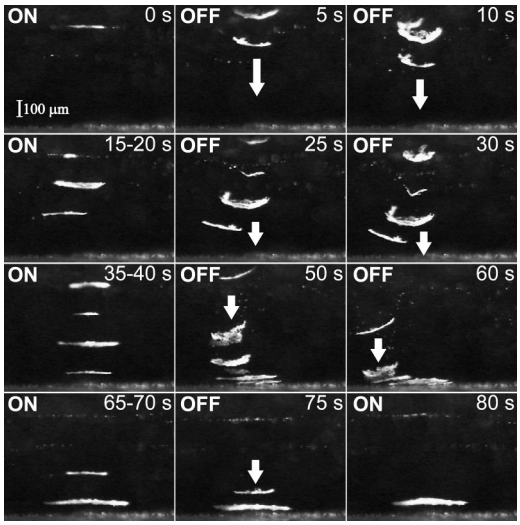

FIG. 5. Side-view demonstration of microsphere collection in the first node 90 μm above the microplate bottom. By turning on and off the acoustic intensity a couple of times during approximately 1 min, all microspheres can be trapped in the lowest node.

To investigate the enrichment efficiency of the UPC, experiments were performed with diluted samples of the 3.2 μm microspheres ($2.5\times10^4\ ml^{-1}$), later used in the TSH-assay measurements. In Fig. 6(a) microscope images of reflected light from ~300 trapped microspheres in four different subsequent pressure nodes (nodes 3–6 from the acoustic lens) are shown, using a 20×/0.5 NA objective. At this low-voltage mode of operation, the microspheres form dense, single-layer aggregates in a very compact arrangement. We believe that this arrangement of the microspheres is optimal for sensitive confocal laser-scanning detection. All fluorescence is concentrated to a minimum area from collected microspheres, all in the focal plane of the scanning laser beam. In contrast to microspheres collected at the bottom of the vessel, all trapped microspheres are surrounded by the buffer solution. Thus, no autofluorescence from the plastic bottom disturbs the measurement and the S/N ratio of the detected fluorescence is maximized. The typical collection time varied from one to a few minutes. The most important factors that affect the collection efficiency are the transducer voltage and the resonator alignment. To obtain statistically significant data, ~100 microspheres must be found and measured. Typically, this can be done in a few minutes at concentration

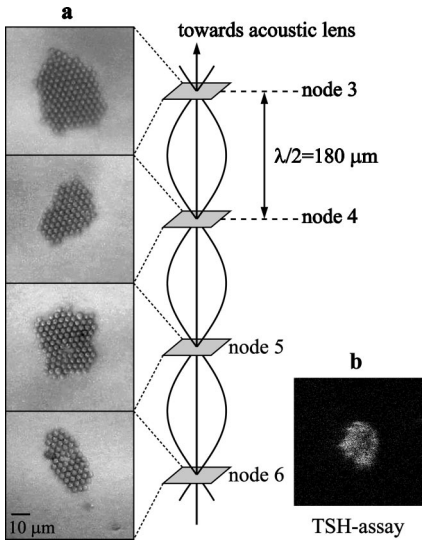

FIG. 6. (a) Reflected light from ~300 collected microspheres in four subsequent pressure nodes, each separated by $\lambda/2=180$ μm. (b) Confocal fluorescence image of the TSH assay from 20 trapped microspheres at 1 mIU/L (with some motion blur due to horizontal movement of the microspheres during the 10 s measurement time).

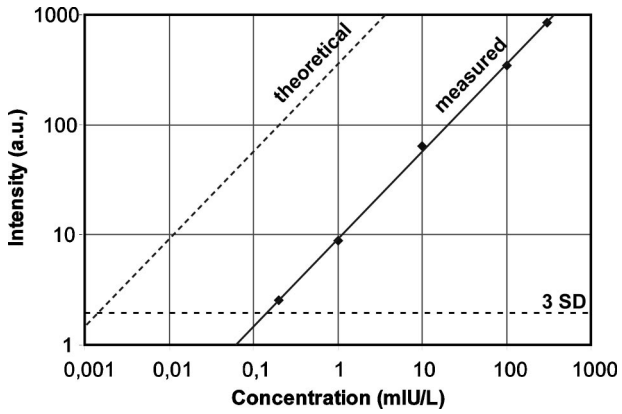

FIG. 7. The TSH assay titration curve. The mean fluorescence intensity per microsphere is calculated from images of trapped microspheres at different concentrations TSH concentrations. The solid line is the measured concentration of the incubated assay, and the dotted line is the theoretical (potential) curve if the 100× dilution after the incubation is taken into consideration.

levels around 10^4 microspheres/ml. When the transducer voltage is increased, the acoustic streaming becomes more significant and only the upper pressure nodes will be useful for microsphere collection. However, in most experiments, we used a low-voltage level ($<5\ V_{pp}$) that resulted in a stable and robust behavior of the UPC with minimum acoustic streaming and medium-rate speed of trapping.

Finally, a high-sensitivity TSH assay was simulated to investigate the potential of the suggested detection method. In this experiment, a comparison with the sensitivity of two-photon excitation (TPX) technology[7] for the same assay was performed. In TPX detection, a typical microsphere concentration is $10^6-10^7\ ml^{-1}$. We prepared the assay with the same coupling protocol as in TPX, but finished by diluting the sample in water, 100× the TPX dilution. This can be regarded as a simulation of an analyte concentration level 100× lower than the limit of the TPX system. Thus, the analyte-to-microsphere ratio is the same, but the analyte concentration in the sample is 100× lower. At this microsphere concentration level, a TPX measurement is no longer practical due to too long measurement time (~hours). A diluted sample of 100 μl containing 2500 microspheres (i.e., 2.5×10^4 spheres/ml) was placed in the vessel, and the FTA was activated at a $5\ V_{pp}$ level. The 20×/0.5 NA objective was used to allow imaging all the pressure nodal planes in the resonator. Typically, 2–3 images were taken from nodes starting at a distance ~400 μm from the vessel bottom. Here, more microspheres were trapped due to lower acoustic streaming in the upper part of the resonator. Since the microspheres moved slightly during the 10 s confocal laser-scanning time, the microscope was switched to wide-field reflected-light mode that allowed for counting the number of trapped microspheres. In Fig. 6(b), a typical confocal laser-scanning fluorescence image of 20 trapped microspheres near the detection limit is shown, from which the intensity was calculated. The scaling is the same as for the images to the left. In Fig. 7, a titration curve of the TSH assay is shown. In the diagram, the curve follows the expected linear scaling to the analyte concentration, and the detection limit is 0.3 mIU/L. This is roughly the same detection limit as of the TPX system.[31] The concentration levels are taken as the actual TSH-assay level before the 100× dilution. Thus, the potential detection limit, providing that the biochemistry is also scalable by 100×, could be down to 100× lower, approaching 0.003 mIU/L (cf. dotted line in Fig. 7).

V. DISCUSSION AND CONCLUSION

Standing-wave ultrasonic trapping and confocal laser-scanning fluorescence detection are two different technologies well-suited for integration in a detection scheme for ultrasensitive biomedical analysis. The ultrasonic particle concentrator (UPC) collects microspheres in plane, dense, single-layer aggregates at well-defined positions controlled by the acoustic resonator geometry and the acoustic frequency, far from the vessel boundary. The layer of trapped microspheres all surrounded by the assay buffer is perfectly compatible with the confocal laser-scanning fluorescence detection. The two major factors that influence the sensitivity of a single-step homogeneous microsphere-based assay are the analyte-to-microsphere ratio and the concentration of microspheres in the sample. As compared to existing technologies, the strength of the UPC-enhanced detection is the possibility to measure samples having extremely low microsphere concentrations. We have shown that the UPC-enhanced method easily can handle samples having microsphere concentrations of $\sim10^4$ spheres/ml. At this concentration level, enough microspheres for a statistically significant analysis can be collected in less than a minute. Although the present proof-of-principle experimental arrangement requires manual adjustment and a total measurement time up to 30 min, the method has potential to be automatized for future high-throughput ultrasensitive analysis.

A fair comparison would be to measure the fluorescence of microspheres on the vessel bottom of the 96-well micro-

plate. Then, the microspheres could be centrifuged down to the bottom before the measurement. This would also allow for the use of high-NA objectives increasing the sensitivity of the measurement. However, even if all microspheres in the sample volume could be centrifuged to the bottom of the vessel, they are still far from each other. For the experiment with 2500 microspheres in 100 μl sample, the packing density is more than 1000 times higher with microspheres trapped by the UPC than microspheres centrifuged down to the bottom. Thus, a typical area of ~100 measured microspheres trapped by the UPC is ten times smaller than the mean area containing a single microsphere centrifuged down to the bottom. This means that the sensitivity improvement the higher NA objectives with short working distances would provide is much smaller than the microsphere packing improvement that the UPC provides. In addition, when measuring on microspheres totally surrounded by liquid and far from the bottom, problems with autofluorescence from the vessel bottom are eliminated. However, there might be a possibility to combine both advantages (i.e., high-NA objectives and UPC) by driving the UPC in the operational mode suggested in Figs. 2(c)–2(e) (the ''trap-sink-retrap'' method). Then, the microspheres will finally be trapped in a plane 50–100 μm above the bottom. This mode of operation was demonstrated with a high-concentration sample of microspheres, but has not yet been investigated in a diluted TSH-assay measurement. It should also be noted that Saito *et al.* have suggested that a similar node integration can be performed by cyclic frequency change,[18] which could be suitable at lower microsphere concentrations.

Our measurements suggest that the potential sensitivity of the method is very high (cf. dotted line in Fig. 7). However, it is difficult to estimate the true limit of detection that is possible to achieve with our suggested method. First, the scaling of the assay when scaling the microsphere is not proportional since the reaction kinetics of the assay is dependent on the microsphere concentration. Moreover, the microsphere concentration efficiency of the UPC is not linear to the microsphere concentration either. The reason is that the acoustic forces from the scattered acoustic field (Bjerknes forces) speed up the rate of trapping. Another concern is the buffer purity. Highly diluted samples require very pure solutions. All kinds of dirt in the sample, protein agglomerations, etc., are easily trapped by the UPC, and if the microsphere concentration is scaled down there is currently a risk that more dirt than microspheres will be trapped. Thus, the surface of the FTA (the acoustic lens) must be very thoroughly cleaned before use. Finally, the lowest theoretical detection limit is always determined by the affinity constant of the antibodies in assay of interest. Still, the potential of the ultrasound-enhanced confocal laser-scanning fluorescence detection is impressive.

VI. SUMMARY

We have combined ultrasonic particle concentration with confocal laser-scanning fluorescence detection for ultrasensitive biomedical analysis using a microsphere-based homogeneous assay. The measured detection limit was 0.3 mIU/L (2 pM) of TSH, but on a sample diluted 100 times after the assay incubation. Thus, the potential (theoretical) detection limit is 0.003 mIU/L (20 fM). Future development includes improvements in the acoustic resonator geometry (thickness matching of all layers) and investigation of the immunoassay reaction kinetics at the femtomolar level.

ACKNOWLEDGMENTS

This work was supported by the Swedish Research Council for Engineering Sciences. The authors thank Mika Kettunen of ArcDia Ltd. for his help with the TSH assay and comparisons with the TPX technology.

[1] P. Hänninen, M. Waris, M. Kettunen, and E. Soini, Biophys. Chem. **105**, 23 (2003).
[2] J. P. Nolan and L. A. Sklar, Trends Biotechnol. **20**, 9 (2002).
[3] E. E. Swartzman, S. J. Miraglia, J. Mellentin-Michelotti, L. Evangelista, and P. M. Yuan, Anal. Biochem. **271**, 143 (1999).
[4] J. Mellentin-Michelotti, L. T. Evangelista, E. E. Swartzman, S. J. Miraglia, W. E. Werner, and P. M. Yuan, Anal. Biochem. **272**, 182 (1999).
[5] C. Martens, A. Bakker, A. Rodriguez, R. B. Mortensen, and R. W. Barret, Anal. Biochem. **273**, 20 (1999).
[6] P. Zuck, Z. Lao, S. Skwish, J. F. Glickman, K. Yang, J. Burbaum, and J. Inglese, Proc. Natl. Acad. Sci. U.S.A. **96**, 11122 (1999).
[7] P. Hänninen, A. Soini, N. Meltola, J. Soini, J. Soukka, and E. Soini, Nat. Biotechnol. **18**, 548 (2002).
[8] E. L. Elson and D. Marge, Biopolymers **13**, 1 (1974).
[9] P. Kask, K. Palo, D. Ullmann, and K. Gall, Proc. Natl. Acad. Sci. U.S.A. **96**, 13756 (1999).
[10] F. J. Meyer-Almes, *Nanoparticle Immunoassays: A New Method for Use in Molecular Diagnostics and High Throughput Pharmaceutical Screening Based on Fluorescence Correlation Spectroscopy*, Fluorescence Correlation Spectroscopy: Theory and Applications, edited by R. Rigler and E. S. Elson (Springer series in Chemical Physics, Berlin, 2000).
[11] S. Schaertl, F. J. Meyer-Almes, E. Lopez-Calle, A. Siemers, and J. Kramer, J. Biomol. Screening **5**, 227 (2000).
[12] M. Gröschl, W. Burger, B. Handl, O. Doblhoff-Dier, T. Gaida, and C. Schmatz, Acust. Acta Acust. **84**, 815 (1998).
[13] S. Gupta and D. L. Feke, Ultrasonics **35**, 131 (1997).
[14] H. M. Hertz, J. Appl. Phys. **78**, 4845 (1995).
[15] E. H. Brandt, Nature (London) **413**, 474 (2001).
[16] W. T. Coakley, Trends Biotechnol. **15**, 506 (1997).
[17] A. Nilsson, F. Petersson, H. W. Persson, H. Jönsson, and T. Laurell, MicroTAS 2002, Nana, Japan.
[18] M. Saito, N. Kitamura, and M. Terauchi, J. Appl. Phys. **92**, 7581 (2002).
[19] N. E. Thomas, M. A. Sobanski, and W. T. Coakley, Ultrasound Med. Biol. **25**, 443 (1999).
[20] S. Bhaskar, J. N. Banavaliker, K. Bhardwaj, and P. Upadhyay, J. Immunol. Methods **262**, 181 (2002).
[21] M. Wiklund, S. Nilsson, and H. M. Hertz, J. Appl. Phys. **90**, 421 (2001).
[22] W. L. Nyborg, J. Acoust. Soc. Am. **42**, 947 (1967).
[23] M. Gröschl, Acust. Acta Acust. **84**, 432 (1998).
[24] L. P. Gorkov, Sov. Phys. Dokl. **6**, 773 (1962) [Dokl. Akad. Nauk SSSR **140**, 88 (1961)].
[25] W. J. Xie and B. Wei, Phys. Rev. E **66**, 026605 (2002).
[26] C. Eckart, Phys. Rev. **73**, 68 (1948).
[27] L. E. Kinsler, A. E. Frey, A. B. Coppens, and J. V. Saunders, *Fundamentals of Acoustics*, 4th ed. (Wiley, New York, 2000).
[28] A. R. Selfridge, IEEE Trans. Sonics Ultrason. **32**, 381 (1985).
[29] M. Hill, Y. Shen, and J. J. Hawkes, Ultrasonics **40**, 385 (2002).
[30] A. Yariv, *Optical Electronics in Modern Communications* (Oxford University Press, Cambridge, 1997).
[31] M. Tirri, J. Vaarno, J. Soini, and P. Hänninen, Opto-Electron. Rev. **11**, 39 (2003).